

Squeezed Light and Entangled Images from Four-Wave-Mixing in Hot Rubidium Vapor

Raphael C Pooser, Vincent Boyer, Alberto M. Marino, Paul D. Lett

Joint Quantum Institute, National Institute of Standards and Technology, University of Maryland, Gaithersburg, MD 20899, USA

ABSTRACT

Entangled multi-spatial-mode fields have interesting applications in quantum information, such as parallel quantum information protocols, quantum computing, and quantum imaging. We study the use of a nondegenerate four-wave mixing process in rubidium vapor at 795 nm to demonstrate generation of quantum-entangled images. Owing to the lack of an optical resonator cavity, the four-wave mixing scheme generates inherently multi-spatial-mode output fields. We have verified the presence of entanglement between the multi-mode beams by analyzing the amplitude difference and the phase sum noise using a dual homodyne detection scheme, measuring more than 4 dB of squeezing in both cases. This paper will discuss the quantum properties of amplifiers based on four-wave-mixing, along with the multi mode properties of such devices.

Keywords: Quantum Imaging, Entanglement, Quantum Optics, Nonlinear Optics

1. INTRODUCTION

The quantum correlations and entanglement present in multi-spatial-mode squeezed fields, which have applications in quantum information and quantum computing, have recently garnered increased general interest. Quantum entanglement in the context of continuous light fields is normally characterized by the fields' quantum fluctuations. Specifically, the quantum fluctuations of a pair of entangled modes (i.e. two-mode squeezed states or twin beams) are correlated to a greater extent than would be possible when observing classical fluctuations. Such states are interesting because of their applicability to quantum information protocols.¹ For multi-spatial-mode twin-beams each beam consists of multiple independent spatial modes. Bipartite entanglement can exist between the independent spatial modes that make up the overall beams, so that many spatial mode pairs are entangled together in parallel. This can give rise to parallel quantum information processing protocols or even squeezing distillation.^{2,3}

Further, multi-spatial-mode beams of light can carry images; storing information in their spatial degrees of freedom. Classically, imaging is thought of as the storage of information in the local mean intensity of a beam. Holographic imaging stores information in the classical phase of the light beam as well. However, one can also consider the local quantum fluctuations of such imaging fields, leading to the concept of quantum imaging.⁴ Quantum imaging is most generally defined as the storage of information in the quantum fluctuations of the phase and amplitude of multiple spatial modes. Accessing the quantum fluctuations of the light yields a higher information density than would be available in a classical image, essentially due to an increased signal to noise ratio stemming from quantum correlations.⁵ Recently, quantum imaging enabled the detection of transverse beam displacements smaller than the standard quantum limit (SQL),⁶ and noiseless image amplification has also been demonstrated.⁸ The prospect of generating these types of light beams is one of the more exciting applications of multi-spatial-mode amplifiers.

This paper will show the generation of quantum images using a nonlinear interaction, four-wave-mixing in rubidium vapor. The next section describes the basic amplifier and its components. The third section characterizes the multi-spatial-mode aspect of the amplifier, and the last section puts this characteristic to use in the generation of entangled images.

Send correspondence to raphael.pooser@nist.gov, paul.lett@nist.gov

2. FOUR WAVE MIXING AMPLIFIER

Four-wave-mixing (4WM) is a nonlinear process based on a third order nonlinearity. Our 4WM scheme is based on a double-lambda system configuration in ^{85}Rb , shown in figure 1. A strong pump field, detuned 800 MHz

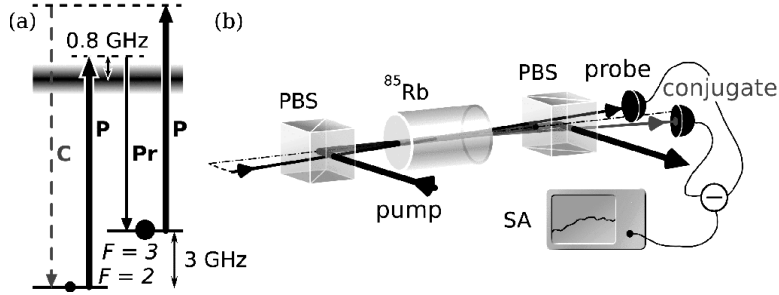


Figure 1. 4WM configuration. (a) Four-level double-lambda scheme in ^{85}Rb , P = pump, C = conjugate, Pr = probe. The width of the excited state represents the Doppler broadened profile. (b) Experimental setup, PBS = polarizing beam splitter, SA = spectrum analyzer. Reproduced from ref. 7.

from the D1 ($5S_{1/2}, F = 2 \rightarrow 5P_{1/2}$) transition in ^{85}Rb (795 nm), and a weak probe beam, detuned 3 GHz to the red of the pump (by the hyperfine ground-state splitting), are input into the vapor cell. The strong third order nonlinearity arises from the coherence built-up between the two hyperfine levels in the ground state. The amplified probe and generated conjugate beams make up the output light fields and have been predicted to exhibit quantum noise reduction.⁹

2.1 Theoretical Two-Mode Quantum Correlations

In general 4WM four electric fields can interact in configurations in which one or more of the fields experience amplification or deamplification inside the nonlinear medium proportional to the magnitude of the nonlinear susceptibility and the amplitude of the interacting fields (in the absence of any other interactions between the light and matter). The nonlinear propagation equations are¹⁰

$$\frac{\partial E_i}{\partial t} = i\kappa_i E_j^* E_k E_l \quad (1)$$

(neglecting other sources of loss and assuming perfect phase-matching), where κ_i is proportional to the third order nonlinear susceptibility.

Similar to systems that have large second order nonlinearities, one can envision configurations based on 4WM that result in quantum correlations between some of the fields. The Heisenberg equations of motion for the field operators are found by quantizing classical nonlinear equations:

$$\dot{a}_i = \chi a_j^\dagger a_k a_l. \quad (2)$$

Typically 4WM schemes involve large field amplitudes input to the nonlinear medium to be used as a pump for the nonlinear interaction (as is true for our configuration). In this situation the pump fields can be considered classical amplitudes, since the gain or loss in the pump fields will be very small relative to the starting amplitudes. In eq. (2) above, if one had two of the fields input as pumps to the nonlinear process, one would be left with:

$$\dot{a}_1 = \kappa a_2^\dagger, \quad (3)$$

$$\dot{a}_2 = \kappa a_1^\dagger, \quad (4)$$

where subscripts 1 and 2 represent two separate amplified fields, for the case in which both pumps are derived from the same electric field. Eqs. (3) and (4) lead to quantum correlations between continuous field variables, specifically linear combinations of the field quadratures. The quadratures themselves are linear combinations

of the raising and lowering operators for the electric fields. One can define a basis with two orthogonal field quadratures:

$$X_i = \frac{1}{\sqrt{2}}(\hat{a}_i + \hat{a}_i^\dagger) \quad (5)$$

$$P_i = \frac{i}{\sqrt{2}}(\hat{a}_i^\dagger - \hat{a}_i), \quad (6)$$

where $i = 1, 2$ corresponds to the two fields amplified by the nonlinear process. Substituting into eqs. (3) and (4) and solving for the quadratures yields

$$P_+(t) = e^{-\kappa t} P_+(0), \quad (7)$$

$$X_-(t) = e^{-\kappa t} X_-(0), \quad (8)$$

where $X_-(t) = X_1(t) - X_2(t)$ and $P_+(t) = P_1(t) + P_2(t)$ are called the generalized quadratures.

The variances of the generalized quadratures decrease as a function of the interaction time in the nonlinear medium:

$$V[X_-(t)] = V[X_-(0)]e^{-2\kappa t}.$$

The variances at $t = 0$ are those of the inputs to the nonlinear medium, typically either the vacuum or a coherent state of nonzero amplitude. Such inputs are minimum uncertainty states whose noise levels define the SQL. The variances exhibit the familiar quantum noise-reduction below the SQL, otherwise called ‘‘squeezing’’. Such noise reduction is often associated with nonlinear interactions based on parametric down conversion (PDC, second order nonlinearity) in either optical parametric amplifiers¹¹ or optical parametric oscillators.¹² The output states are the familiar two-mode squeezed states (so-called because the noise reduction is a property of a joint variable of the two fields). In the case of 4WM, for every two pump photons that are annihilated in the nonlinear medium, a single photon is emitted into each of the two output fields simultaneously. This leads to correlations between the intensities of the output beams to better than would be allowed by the SQL. In other words, one should observe squeezing on the intensity difference between the output fields.

In fact, squeezing was first observed in 4WM by Slusher et al.¹³ Since then, noise reduction in 4WM has been observed under various conditions.^{14–23} However, the amount of squeezing had not exceeded 2.2 dB²³ until recently.²⁴ Our scheme has output states which exhibit up to 8 dB of intensity-difference noise reduction, shown in the next section.

2.2 Intensity-Difference Noise Reduction

Light amplified by the 4WM scheme shown in figure 1 can be described by equations (3) and (4). A strong pump beam (400 mW) with a 500 μm waist and a weak probe (100 μW) with a 250 μm waist are input at a small angle ($\theta \sim 0.75^\circ$) so that they overlap throughout the 12.7 mm length of the vapor cell. The cell is heated to 110 $^\circ\text{C}$ to increase the Rb number density (vapor pressure). The probe field is generated by splitting the pump and passing part of it through an acousto-optic modulator to downshift its frequency by 3 GHz. As a result the phase difference between the pump and probe is stable.

In this configuration, the probe field experiences a gain, G , and is amplified, while the conjugate field is amplified from the vacuum (see fig. 1a). The field operators for the probe and conjugate transform as follows in the gain region:

$$a_1 \rightarrow a_1 \sqrt{G} - a_2^\dagger \sqrt{G-1} \quad (9)$$

$$a_2^\dagger \rightarrow a_2^\dagger \sqrt{G} - a_1 \sqrt{G-1}, \quad (10)$$

where G depends on the strength of the interaction: $\sqrt{G} = \cosh \kappa t$, $\sqrt{G-1} = \sinh \kappa t$. When the probe port a_1 is seeded with a coherent state $|\alpha\rangle$ and the conjugate port a_2 is fed with the vacuum, the output intensity-difference noise is equal to the shot noise of the input, which gives a quantum noise reduction of $1/(2G-1)$ with respect to the output SQL. Thus, we expect that for a perfect amplifier the squeezing increases with increasing gain.

In reality, losses in the atomic medium limit the squeezing somewhat, as the probe experiences more absorption than the conjugate since it is tuned closer to resonance. A distributed gain/loss model (discussed elsewhere⁷) accurately predicts the amount of squeezing we measure in the output of our amplifier.

As shown in figure 1b, in our experiment the pump is separated from the probe and conjugate signal fields on a polarizing beam splitter, and the probe and conjugate intensities are detected separately and then subtracted. The difference signal shows the noise power of the intensity-difference when viewed on a spectrum analyzer. Figure 2 below shows that 8 dB of noise reduction below the SQL is possible with our amplifier system.⁷ The actual squeezing bandwidth is approximately 20 MHz (not shown in fig. 2).

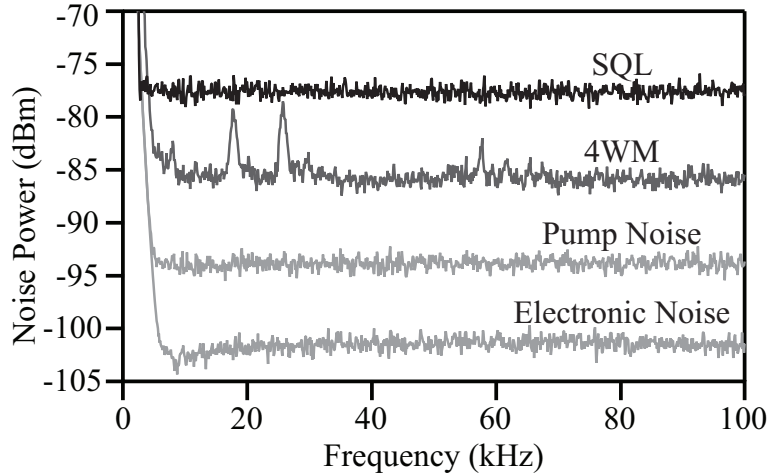


Figure 2. Intensity-difference squeezing. Noise spectra (RBW=1 kHz, VBW=10 Hz) for the electronic noise, the scattered pump light, the intensity-difference, and the standard-quantum limit. Reproduced from ref. 7.

Section 2.1 suggests that in addition to the intensities being correlated, the orthogonal quadratures of the two fields should also exhibit the same degree of quantum correlations, a property of phase-insensitive amplifiers.²⁵ Further, the presence of such correlations in both the X_- and P_+ quadratures (which can be associated with the intensity-difference and phase-sum) indicates the presence of entanglement between the output fields.²⁵

2.3 Continuous Variable Entanglement

In order to observe entanglement the noise reduction in the two generalized quadratures must satisfy the inseparability criterion: $I = \langle \Delta X_-^2 \rangle + \langle \Delta P_+^2 \rangle < 2$.^{26,27} Several other systems have been used to demonstrate inseparability: optical parametric oscillators below^{28,29} and above^{30,31} threshold, 4WM in optical fibers,³² and mixing of single-mode squeezed states.³³

To demonstrate the entanglement between the probe and conjugate fields of our amplifier, the quadratures of both fields need to be detected simultaneously. Both signal field quadratures are detected using homodyne detectors, and the difference and sum of the two detectors give access to the variances of the generalized quadratures X_- and P_+ from section 2.1, which are needed to verify the inseparability criterion.

In our case, the signal fields are non-degenerate and require two phase-locked local oscillators (LOs) with frequencies separated by 6 GHz. To produce the signals and LOs we seed two 4WM processes inside the same ⁸⁵Rb vapor cell. In the first 4WM interaction we inject only the pump into the cell and seed the probe and conjugate ports with the vacuum. In the second we inject the pump and also a small seed (100 μ W) on the probe port. We use this second 4WM interaction to produce the local oscillators which are used in the homodyne detectors that measure the field quadratures output by the first (unseeded) 4WM process. This method of generating the LOs eliminates problems that might otherwise limit mode matching. For instance, a cross-Kerr

modulation causes a lensing effect inside the cell that is different for the probe and conjugate and depends on the pump intensity. Any change in the parameters would require a change in the mode matching optics for the LOs if they were not derived from the same 4WM process. Having the LOs undergo the same Kerr-lensing as the signals eliminates this problem. Further, since the LOs are derived from a 4WM process that is driven by the same pump laser as for the signal fields, their phase difference with the signals is stable, which eliminates the need to actively stabilize the LO phases.

The signal fields themselves consist of two-mode squeezed vacuum states, where “two-mode” entails the two separate output fields, one at the probe frequency and the other at the conjugate frequency. The generalized quadratures for the two-mode squeezed vacuum output fields should exhibit the noise properties discussed in section 2.1, which outlines noise properties of the amplifier for either coherent state or vacuum input. The advantages of using two-mode squeezed vacuum as the signal are apparent in the requirement that the local oscillator power be much larger than the analyzed field in homodyne detection. Our LOs consist of 500 μW typically. Further advantages will be evident in later sections when multi-spatial-mode entanglement is discussed.

In order to align the homodyne detectors, the the 4WM process for the signals is first seeded with a small input ($\sim 100\mu\text{W}$) so that the output fields are comprised of bright beams. This provides a visual guide for alignment on the beamsplitters. After optimizing the interference between the LOs and signals on the beamsplitters, the seed is blocked so that the signal fields consist of two-mode-squeezed vacuum. This alignment procedure insures that the vacuum modes that are analyzed in the homodyne detectors are the correct spatial modes to analyze in order to observe entanglement. In other words, overlapping the LOs with a bright two-mode-squeezed state output from the cell beforehand insures that the the vacuum modes analyzed in the homodyne detectors also belong to the same two-mode-squeezed vacuum state.

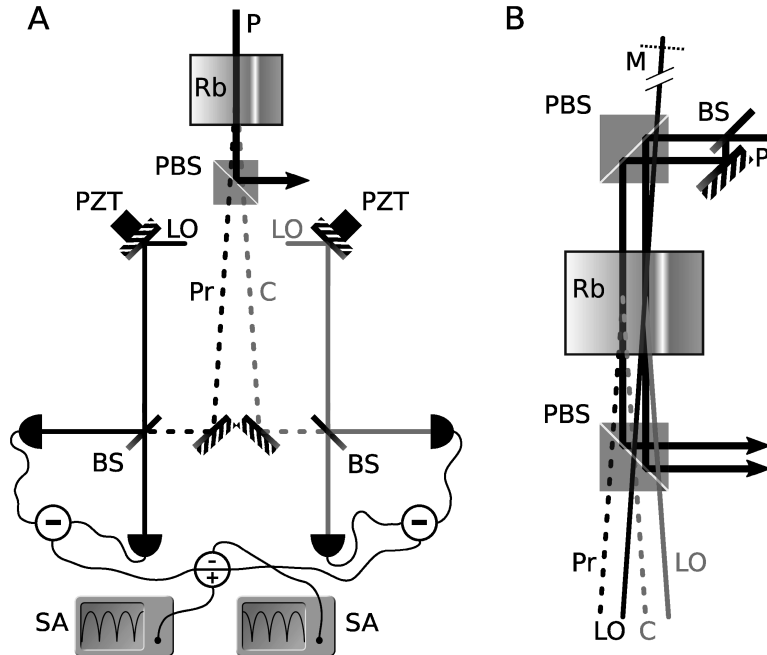


Figure 3. A: Setup of the homodyne detection. P: pump, Pr: probe, C: conjugate, LO: local oscillator, BS: 50/50 beamsplitter, PBS: polarizing beamsplitter, PZT: piezoelectric actuator, Rb: rubidium vapor cell, SA: spectrum analyzer. B: Generation of the LOs used in the homodyne detectors. Reproduced from ref. 34.

Figure 3b shows the generation of local oscillator fields and vacuum squeezed fields. Figure 3a shows the homodyne detection scheme. One of the mirrors in each of the local oscillator beam paths is mounted on a piezoelectric device. The piezoelectric actuators are scanned synchronously so that the relative phases between the local oscillators and the signal fields are scanned in unison, insuring that the homodyne detectors measure

the same quadratures for the two signal fields at any given time. The homodyne detector signal as a function of local oscillator phase gives a generalized quadrature: $A_\theta = X \cos \theta + P \sin \theta$. A hybrid junction outputs the sum and difference of the two homodyne detector signals, which are recorded simultaneously on two spectrum analyzers. At a local oscillator phase of zero radians, the difference signal between the homodyne detectors measures X_- , while at a phase of $\pi/2$ the sum of the signals measures P_+ .

As the LO phases are scanned, the measured quadratures show correlations or anti correlations in their sum and difference. Figure 4 shows the sum and difference of the detector signals as a function of spectrum analyzer sweep time, which amounts to the local oscillator phase. At one point the noise power of the difference signal is minimized, while the noise of the summed signal is maximum. At a later time the signals are reversed. The two noise powers switch places at equal intervals as a function of local oscillator phase: when one signal is minimized, the other is always maximized. This indicates that the two homodyne detectors are measuring the same quadrature for both signal fields, and that the generalized quadratures being measured at the minima of each curve are equivalent to the X_- and P_+ of section 2.1.

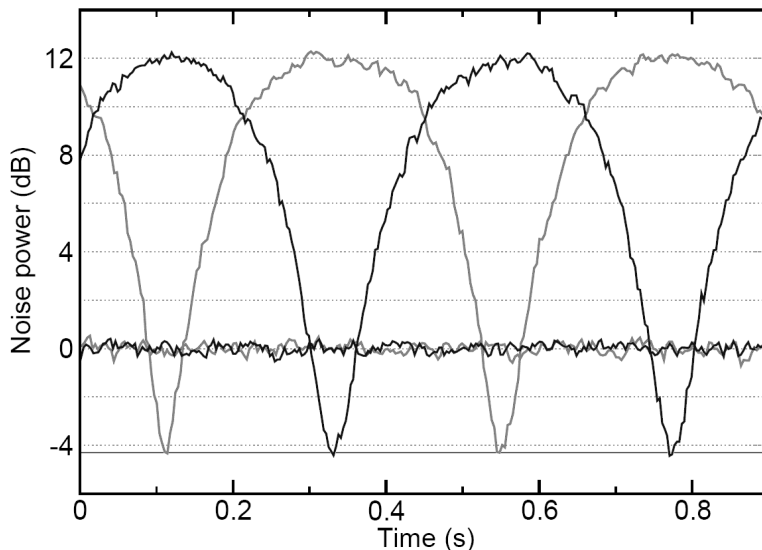


Figure 4. Noise power for the generalized quadratures as a function of local oscillator phase scan. The dark line is the difference between the homodyne detectors and its minima represent the X_- quadrature. The gray line shows the summed signal and its minima represent the P_+ quadrature. Reproduced from ref. 34.

Figure 4 shows noise reduction of -4.3 ± 0.2 dB* in each quadrature.³⁴ This translates to an inseparability value of $I = 0.74 \pm 0.02$, which fulfills the inseparability criterion $I < 2$. The overall detection efficiency was $90 \pm 3\%$. The seed for the LOs used for these measurements were simple gaussian beam profiles. The next section discusses exploiting the multi-mode nature of the amplifier to produce multi-spatial mode entangled beams.

3. MULTI-SPATIAL-MODE AMPLIFICATION

Up to now most of the discussion has not made a distinction between the idea of single-spatial-mode or multi-spatial-mode amplifiers. In fact, the common thread between each of the systems mentioned at the beginning of section 2.3 is that they involve single-spatial-mode operation. In other words, the signal fields each occupy a single mode of the electromagnetic field, being generated either inside an optical resonator cavity or a single-mode optical fiber. Thus, the entanglement generated by these systems is generally between two distinct modes. In many cases, this is a desirable effect. For instance, a single spatial mode is more easily mode-matched back

*All uncertainties quoted in this paper represent one standard deviation, combined statistical and systematic uncertainties.

into another cavity or optical fiber than a multi-spatial-mode field would be. This inherent strength also makes these systems difficult to use for quantum imaging, however, where multi-spatial-mode amplification is needed.

The 4WM amplifier we present here does not use a cavity to enhance the nonlinear gain, and aside from temperature control otherwise consists of only a simple vapor cell. Since no mode-matching is required in order to couple the pump and probe into the amplifier, the spatial modes of the amplifier are determined by the spatial-phase-matching bandwidth of the gain medium.³⁵ The probe, therefore, can seed several spatial modes of the amplifier at once. In the special case where the probe input field is a single mode, the output would still be multi-mode since the 4WM process would amplify all of the vacuum modes surrounding the input probe, so that the output state would consist of many amplified spatial modes regardless of which modes the probe seeds.³⁶

One indication of multi-mode behavior is that the amplifier has appreciable gains for a range of angles between the pump and probe. In the case of the forward 4WM geometry used here, the angle between pump and seed is usually a stringent condition.³⁷ For our amplifier, this condition is relaxed by two factors. First, in the absence of dispersion the phase-matching would normally command all the beams to be collinear, but the appearance of a strong dispersion of the index of refraction for the probe³⁸ allows the existence of a pair of frequencies for the pump and the probe such that the 4WM gain is maximum for a non-zero θ , around $\theta_0 = 7$ mrad. Second, large gain allows us to use a relatively thin nonlinear medium. This relaxes the phase-matching condition since the length of the gain medium is shorter than the coherence length of the nonlinear interaction. This effectively quasi-phase-matches a range of angles (the shorter the cell, the larger the range of quasi phase-matched angles). All spatial modes within the angular bandwidth can be amplified simultaneously, and quantum correlations can be generated on many spatial mode pairs at the same time.

Figure 5 shows the gain and intensity-difference squeezing as a function of angle between the pump and probe. The width of the squeezing curve gives an approximate angular acceptance bandwidth of $\Delta\theta \approx 8$ mrad. Essentially, any input spatial modes that fall within this angular acceptance bandwidth will be amplified.

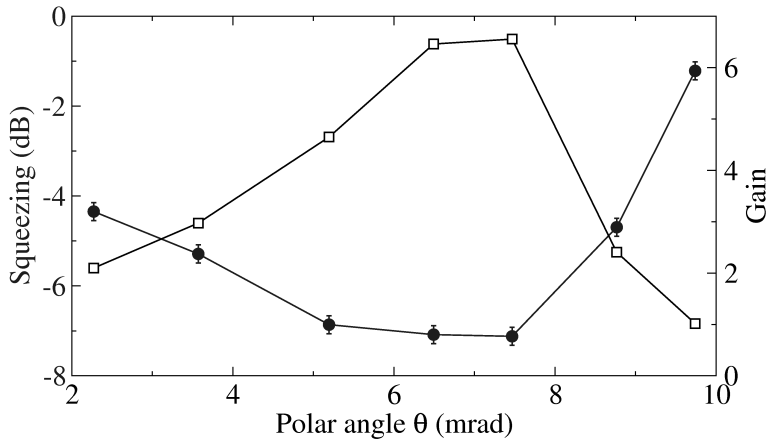


Figure 5. Gain (\square) and intensity-difference noise reduction (\bullet) as a function of angle θ . Reproduced from ref. 36.

A way to verify the size of an amplified mode in the far field, or determine the “resolution” of the amplifier, is to seed the amplifier with a probe whose waist is much larger than the pump inside the amplifying medium. This means that the spread of k-vectors for the probe is smaller than that of the pump. The corresponding conjugate will have a diameter much smaller than the input probe in the far field, limited by the inverse transverse size of the pump in the gain medium. Under these conditions, the transverse size of the conjugate is approximately 1 mrad for our amplifier. The number of spatial modes that the amplifier supports is then the number of 1 mrad beams that fit into the solid angle of acceptance. From figure 5, the acceptance solid angle is the cone that extends from 2 mrad to 10 mrad, thus the total number of spatial modes supported by the amplifier is of the order of 10^2 .

3.1 Multi-Spatial-Mode Intensity-Difference Noise Reduction

A more striking demonstration of the amplifier’s multi-mode nature would be an imaging experiment. Placing an opaque mask in the probe beam path before the vapor cell changes the shape of the input beam from a Gaussian to that of a spatially-modulated beam (image). As long as the image formed by the mask fits into the spatial bandwidth of the amplifier, the image should be amplified, and a conjugate image should be generated. Figure 6 shows the input and output of the amplifier for one such mask. Here, the mask cuts the intensity of the probe such that the input to the amplifier looks like the letters “N T”.

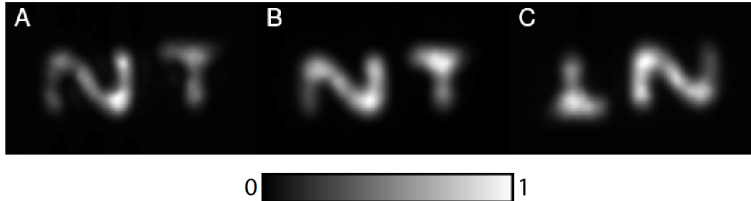


Figure 6. Intensity-difference squeezing in the multi-spatial-mode regime. The images were captured by projecting the beams onto a screen in the far field and capturing the images on the screen with a CCD camera. (A) is the image of the probe seed in the far field, (B) is the image of the output probe in the intermediate field, and (C) is the image of the conjugate in the far-field. The intensities are normalized to 1. The different optical conjugation distances for the probe and the conjugate images show the lensing effect due to the cross-Kerr interaction with the pump beam, which acts mostly on the probe. Reproduced from ref. 34.

Measuring the intensity-difference between the probe and conjugate the same way as for Gaussian beam profiles in earlier sections showed that the probe and conjugate intensities were correlated with -5.4 ± 0.2 dB of intensity-difference noise reduction.³⁴ Thus, the “N T” probe and conjugate images were intensity-difference-squeezed. Next, a spatial filter (razor blade) was applied to the output images. The T in each image was blocked so that the detectors measured the intensity of only the N parts of the image. The intensity-difference between the N parts was found to be squeezed by -5.2 ± 0.2 dB.³⁴ When blocking the N parts and measuring the intensity-difference of the T parts, the noise reduction was found to be -5.1 ± 0.2 dB.³⁴ Measuring the difference while blocking the N in one beam and blocking the T in the other would yield excess noise,³⁶ which means that the correlations between images are localized to parts with similar details. Having generated the “N T” image using a single input beam, the presence of independent correlations between subparts of the output image proves that the amplifier is multi-spatial-mode.^{39,40} It should be pointed out that the subparts of the “N T” image were independently correlated at sufficiently high analyzer frequencies (> 3.5 MHz), but at lower frequencies cross-talk was present. In other words, below a 3.5 MHz analyzer frequency, blocking the T would degrade the squeezing measured between the remaining N subparts. Nonetheless, independent correlations were observed between subparts for certain analysis frequencies. Study of the cross-talk effect is beyond the current scope and will be discussed elsewhere.

The independence of the correlations between subparts of the image is not unexpected. The noise properties of the amplifier discussed in earlier sections dealt with single spatial modes of the electromagnetic field. However, the 4WM amplifier presented here can be thought of as many single-spatial mode amplifiers working in parallel. All modes within the spatial bandwidth of the amplifier are amplified simultaneously, and pairs of spatial modes exhibit the noise properties discussed in section 2.1. In this context, the “N T” image is clearly a superposition of spatial amplifier modes. Thus the output images in fact consist of many subparts that are independently correlated. The size of these correlated subparts is probably well-approximated by the 1 mrad beam size given at the beginning of this section.

Lastly, if the multi mode amplifier exhibits intensity-difference noise reduction, it follows from previous sections that the amplifier output states also exhibit entanglement for multiple spatial modes simultaneously. The next section discusses the generation of quantum-entangled images.

4. QUANTUM-ENTANGLED IMAGES

To detect entanglement between multi-spatial-mode beams, or image-carrying beams, the experiment of section 2.3 was repeated with a mask in the beam path of the seed used to generate the LOs. The LO shape selects which two-mode-squeezed vacuum modes the homodyne detectors measures. Changing the angle, size, or general shape of the LO beam all have an effect on exactly which spatial modes are analyzed. However, as long as the LO beams fit within the spatial bandwidth of the amplifier, there will always be a set of two-mode-squeezed vacuum modes that the bright part of the LOs can overlap with and analyze in the homodyne detectors. In general, this means that an arbitrary local oscillator shape can be used to interrogate the signal fields, as long as the LOs overlap the correct vacuum modes in the homodyne detectors for both the probe and conjugate, as discussed in section 2.3.

A mask was placed in the seed beam path which imprinted the image of a letter “T” onto the seed and subsequently both LOs. Figure 7 shows the results of the homodyne detection measurements for this case, along with the actual LO images at the homodyne detectors.

Figure 7 shows -3.6 ± 0.2 dB of noise reduction in each generalized quadrature.³⁴ This again satisfies the inseparability criterion. Therefore, we have shown that an arbitrarily shaped local oscillator can be used in order to measure the entanglement in our system. This means that the system is inherently multi mode, and arbitrary images, within the spatial bandwidth of the 4WM process, can be amplified as quantum-entangled images. As a further example we show below in figure 8 the output images when we use a “cat face” mask on the input. The recorded noise reduction is -1 dB in each quadrature, showing that the entire images are entangled with one another between the two-mode-squeezed vacuum signal beams.

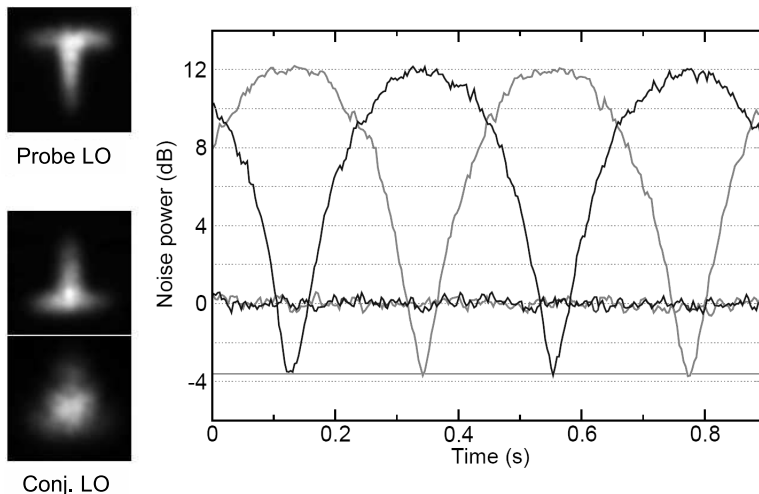


Figure 7. Noise power for the generalized quadratures as a function of local oscillator phase scan. The dark line is the difference between the homodyne detectors and its minima represent the X_- quadrature. The gray line shows the summed signal and its minima represent the P_+ quadrature. The images on the left show the LOs at the homodyne detector. The conjugate image is shown twice, once near the homodyne detector where it appears distorted and once in the far field. The difference between the images at the homodyne detectors arises from the fact that the probe and conjugate experience different Kerr-lensing effects in the nonlinear medium, and thus have different image planes. Reproduced from ref. 34.

5. CONCLUSION

In this paper we have discussed the quantum noise properties of our phase-insensitive 4WM amplifier system, and we have shown that the device amplifies and entangles multiple spatial modes simultaneously. Further, we have shown that our 4WM amplifier can be used for quantum imaging by demonstrating entanglement between multiple spatial modes in the form of images. The subparts of the images, or smaller details, are also

independently correlated. Future work will involve characterizing how the nature of the entanglement of smaller details changes as the various parameters of our system change.

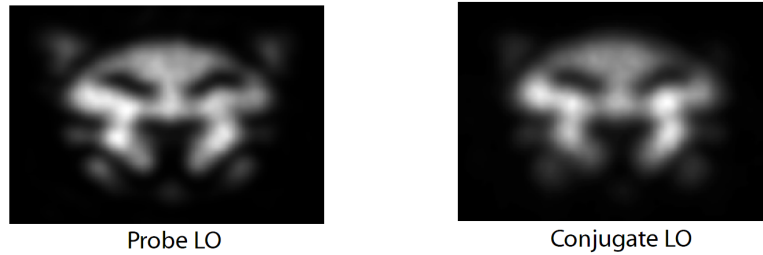


Figure 8. Images of the local oscillators used to measure entanglement in a “cat face” mode. The squeezing was -1 dB in each quadrature. Reproduced from ref. 34.

REFERENCES

- [1] S. L. Braunstein, P. van Loock, *Rev. Mod. Phys.* **77**, 513 (2005).
- [2] A. Franzen, B. Hage, J. DiGuglielmo, J. Fiurásěk, and R. Schnabel, *Phys. Rev. Lett.* **97**, 150505 (2006).
- [3] J. Heersink, Ch. Marquardt, R. Dong, R. Filip, S. Lorenz, G. Leuchs, and U.L. Andersen, *Phys. Rev. Lett.* **96**, 253601 (2006).
- [4] M. I. Kolobov, ed., *Quantum imaging* (Springer, New York, 2007).
- [5] M. I. Kolobov, C. Fabre, *Phys. Rev. Lett.* **85**, 3789 (2000).
- [6] N. Treps, et al., *Science* **301**, 940 (2003).
- [7] C. F. McCormick, A. M. Marino, V. Boyer, P. D. Lett, arXiv:quant-ph/0703111v2
- [8] A. Mosset, F. Devaux, E. Lantz, *Phys. Rev. Lett.* **94**, 223603 (2005).
- [9] M. D. Lukin, P. R. Hemmer, and M. O. Scully, *Adv. At. Mol. Opt. Phys.* **42**, 347 (2000).
- [10] Robert W. Boyd, *Nonlinear Optics* (Academic Press, New York, 1992).
- [11] A. Heidmann et al., *Phys. Rev. Lett.* **59**, 2555 (1987).
- [12] S. Feng and O. Pfister, *Phys. Rev. Lett.* **92**, 203601 (2004).
- [13] R.E. Slusher, L.W. Hollberg, B. Yurke, J.C. Mertz, J.F. Valley, *Phys. Rev. Lett.* **55**, 2409 (1985).
- [14] M.W. Maeda, P. Kumar, J.H. Shapiro, *Opt. Lett.* **12**, 161 (1987).
- [15] L.A. Orozco, M.G. Raizen, M. Xiao, R.J. Brecha, H.J. Kimble, *J. Opt. Soc. Am. B* **4**, 1490 (1987).
- [16] M.G. Raizen, L.A. Orozco, M. Xiao, T.L. Boyd, H.J. Kimble, *Phys. Rev. Lett.* **59**, 198 (1987).
- [17] M. Vallet, M. Pinard, G. Grynberg, *Europhys. Lett.* **11**, 739 (1990).
- [18] S.T. Ho, N.C. Wong, J.H. Shapiro, *Opt. Lett.* **16**, 840 (1991).
- [19] D.M Hope, H.-A. Bachor, P.J. Manson, D.E. McClelland, P.T.H. Fisk, *Phys. Rev. A* **46**, R1181 (1992).
- [20] V. Josse, A. Dantan, L. Vernac, A. Bramati, M. Pinard, E. Giacobino, *Phys. Rev. Lett.* **91**, 103601 (2003).
- [21] J. Ries, B. Brezger, A.I. Lvovsky, *Phys. Rev. A* **68**, 025801 (2003).
- [22] M.T.L. Hsu, G. Hétet, A. Peng, C. Harb, H.-A. Bachor, M.T. Johnsson, J.J. Hope, P.K. Lam, A. Dantan, J. Cviklinski, A. Bramati, M. Pinard, *Phys. Rev. A* **73**, 023806 (2006).
- [23] A. Lambrecht, T. Coudreau, A.M. Steinberg, E. Giacobino, *Europhys. Lett.* **36**, 93 (1996).
- [24] C. F. McCormick, V. Boyer, E. Arimondo, P. D. Lett, *Opt. Lett.* **32**, 178 (2007).
- [25] M. D. Reid, P. D. Drummond, *Phys. Rev. Lett.* **60**, 2731 (1988).
- [26] L.-M. Duan, G. Giedke, J. I. Cirac, P. Zoller, *Phys. Rev. Lett.* **84**, 2722 (2000).
- [27] R. Simon, *Phys. Rev. Lett.* **84**, 2726 (2000).
- [28] Z. Y. Ou, S. F. Pereira, H. J. Kimble, K. C. Peng, *Phys. Rev. Lett.* **68**, 3663 (1992).
- [29] J. Laurat, T. Coudreau, G. Keller, N. Treps, C. Fabre, *Phys. Rev. A* **70**, 042315 (2004).
- [30] A. S. Villar, L. S. Cruz, K. N. Cassemiro, M. Martinelli, P. Nussenzveig, *Phys. Rev. Lett.* **95**, 243603 (2005).
- [31] J. Jing, S. Feng, R. Bloomer, O. Pfister, *Phys. Rev. A* **74**, 041804 (2006).

- [32] C. Silberhorn, et al., Phys. Rev. Lett. **86**, 4267 (2001).
- [33] H. Yonezawa, S. L. Braunstein, A. Furusawa, Phys. Rev. Lett. **99**, 110503 (2007).
- [34] V. Boyer, A. M. Marino, R. C. Pooser, and P. D. Lett, Science, 12 June 2008 (DOI: 10.1126/science.1158275).
- [35] Jedrkiewicz et al., Phys. Rev. Lett. **93**, 243601 (2004).
- [36] V. Boyer, A. M. Marino, and P. D. Lett, Phys. Rev. Lett., **100**, 143601 (2008).
- [37] P. Kumar, M. I. Kolobov, Opt. Comm. **104**, 374 (1994).
- [38] V. Boyer, C. F. McCormick, E. Arimondo, and P. D. Lett, Phys. Rev. Lett. **99**, 143601 (2007).
- [39] M. I. Kolobov, Rev. Mod. Phys. **71**, 1539 (1999).
- [40] P. Navez, E. Brambilla, A. Gatti, L. A. Lugiato, Phys. Rev. A **65**, 013813 (2001).